J Mater Sci: Mater Electron (2015) 26:6848–6852
DOI 10.1007/s10854-015-3300-0

Effects of annealing temperature on the magnetic properties of $ZnFe_{1.97}Eu_{0.03}O_4$ nanoparticles

Lili Yang[1] · Donglai Han[2,3] · Hongbo Liu[1] · Yang Liu[1] · Shuo Yang[2,3] · Zhe Wang[1] · Bayanheshig[2]

Received: 13 January 2015 / Accepted: 1 June 2015 / Published online: 9 June 2015

Abstract The $ZnFe_{1.97}Eu_{0.03}O_4$ nanoparticles were prepared with sol–gel method. The effects of sintering temperature on the structural, morphological and magnetic properties were investigated in detail. The results revealed that the $ZnFe_{1.97}Eu_{0.03}O_4$ NPs exhibited weak ferromagnetic properties due to the formation of defects in $ZnFe_2O_4$ caused by Eu^{3+} doping. Moreover, the increased sintering temperature not only enlarged the grain size but also decreased the magnetization of $ZnFe_{1.97}Eu_{0.03}O_4$ NPs due to the decrease of defects in the crystal lattices.

1 Introduction

In recent years, the ferrites (AFe_2O_4) nanostructures have attracted much attention since they can be used as magnetic recording materials, microwave devices, humidity sensors, and pigments [1–4]. Among AFe_2O_4, zinc ferrite ($ZnFe_2O_4$) are well-known to possess various properties such as magnetic behavior [5–8], electrical characteristics [9], semiconductor photocatalysis [2, 10], absorbent material for hot-gas desulfurization [11, 12], and so on. The magnetic properties of $ZnFe_2O_4$ nanostructures vary greatly with their chemical structures, which is strongly depending on the dopant, size and synthesis conditions [5–8]. So people can tailor their magnetic properties by controlling the species and the amounts of different substitutes [13, 14].

Normally, the as-prepared $ZnFe_2O_4$ nanostructures present the paramagnetic property. To make them exhibit ferromagnetic properties, people usually doped transition metals (Mn, Ni, etc.) impurities into $ZnFe_2O_4$ [15, 16]. Since rare earth (RE) ions play an important roles in determining the magneto-crystalline anisotropy in 4f-3d inter-metallic compounds [17, 18], we can deduce that doping small amount of rare earth with larger radius into the $ZnFe_2O_4$ can bring an important modification for both structural and magnetic properties. While, so far only a few works tried to dope RE ions into $ZnFe_2O_4$ to improve their structural and magnetic properties [19–24]. For instance, Rezlescu et al. pointed out that RE ions could drastically affect the physical properties of substituted ferrites due to their larger ionic radius, and when the doping contents of RE ions were relatively low, the RE ions could enter into the octahedral sites (B-sublattice) of Zn ferrites, and replace Fe^{3+} ions in the lattice [19, 20]. Among the RE ions, we are quite interested in the europium element since few research has been reported about the europium doping effects on the magnetic properties of $ZnFe_2O_4$.

The sol–gel method is a very popular route for the preparation of nanoparticles, which is considered as a facile route with a relatively low temperature and low cost. People took this method to prepare Ni–Zn ferrite nanoparticles [25, 26], Mn–Zn ferrite powders [27], NiCuZn ferrite films [28]. For this method, the sintering temperature generally has great influence on the structure and magnetic properties of samples. However, the investigation on the sintering effects is rarely reported. Therefore, in this work, we synthesized the $ZnFe_{1.97}Eu_{0.03}O_4$ nanoparticles by sol–gel method and investigated the effect

✉ Lili Yang
jsdxyll@163.com

[1] Institute of Chemistry and Chemical Engineering, Jiangsu University, Zhenjiang 212013, China

[2] Changchun Institute of Optics Fine Mechanics and Physics, Chinese Academy of Sciences, Changchun 130033, China

[3] University of Chinese Academy of Sciences, Beijing 100049, China

of sintering temperature on the structure and magnetic performance of the samples. The influence mechanism was also discussed in detail.

2 Experimental

2.1 Synthesis

$ZnFe_{1.97}Eu_{0.03}O_4$ nanoparticles were synthesized via the sol–gel method. For $ZnFe_{1.97}Eu_{0.03}O_4$ nanoparticles, the citric acid (CA), $Zn(NO_3)_2{\cdot}6H_2O$ and $Fe(NO_3)_3{\cdot}9H_2O$ were firstly dissolved in 200 mL deionized water with a molar ratio of 3:1:2. The Eu_2O_3 powder was dissolved in 0.1 mol/L dilute nitric acid to form europium nitrate aqueous solution. Then this europium nitrate was added into the above mixture with a Zn:Eu molar ratio of 1:3. The mixture was magnetic stirring for 24 h at room temperature. Then the solution was kept in a dry cabinet at 80 °C for 48 h to obtain $ZnFe_{1.97}Eu_{0.03}O_4$ gel. After that, we further adjusted the dry cabinet to 120 °C and kept the gel in it for 24 h to obtain the xerogel. Herein, we obtained the precursor of the sample.

In order to investigate the influence of sintering temperature on structural and magnetic properties, as-prepared precursor was sintered at 400, 550, 650, 750 °C for 2 h in air to get the final $ZnFe_{1.97}Eu_{0.03}O_4$ nanoparticles, respectively.

2.2 Characterization

X-ray diffraction (XRD) patterns were recorded by a MAC Science MXP-18 X-ray diffractometer with Cu target as radiation source. The scanning electron microscope (SEM, S-570, Hitachi) with an energy dispersive spectrometer (EDS) was used to characterize the morphology and different chemical composition of the samples. The transmission electron microscope (TEM, JEM-2100, JEOL) spectroscopy system was used to qualitatively confirm the detailed microscopic structure. A quantitative compositional analysis was carried out by using an X-ray photoelectron spectroscopy (XPS) in an ultra-high vacuum chamber at a pressure lower than 1.333×10^{-7} Pa. The magnetic properties of the samples were measured by a Lake Shore 7407 vibrating sample magnetometer (VSM).

3 Results and discussion

Figure 1 showed XRD patterns of $ZnFe_{1.97}Eu_{0.03}O_4$ nanoparticles sintered at different temperatures. All the patterns can be readily indexed to cubic $ZnFe_2O_4$ with spinel structure (JCPDS file No. 79-1150), where the

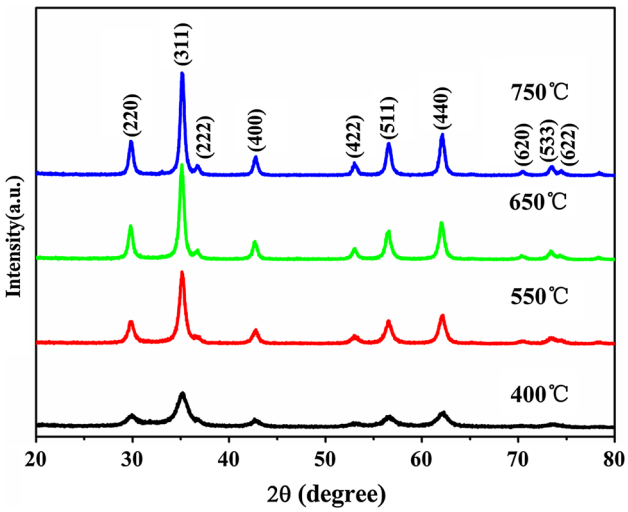

Fig. 1 XRD patterns of $ZnFe_{1.97}Eu_{0.03}O_4$ nanoparticles sintered at 400, 550, 650 and 750 °C

diffraction peaks at 2θ values of 29.8°, 35.09°, 42.74°, 56.5°, and 62.07° could be ascribed to the reflection of (220), (311), (400), (511) and (440) planes, respectively. For all samples, no diffraction peaks were detected from europium oxides, which indicates that Eu^{3+} ions successfully incorporated into $ZnFe_2O_4$ matrix. With increasing the sintering temperature, we can find that the diffraction peaks turned narrower and narrower, which indicated the crystallization of the sample became better gradually.

To study the effect of the sintering temperature on the grain size of the samples, we calculated their average grain size with Scherrer equation:

$$D = \frac{0.89\lambda}{\beta \cos\theta} \quad (1)$$

where D is particle size, λ is wavelength of the X-ray radiation, θ is Bragg's angle, and β is the full width at half maximum (FWHM) of diffraction peaks. According to the Eq. (1), the average grain size of $ZnFe_{1.97}Eu_{0.03}O_4$ was 12, 14, 16, 17 nm corresponding to the sintering temperature of 400, 550, 650 and 750 °C, respectively. Obviously, the grain sizes of the samples increased step by step with the increase of the sintering temperature [29].

To further reveal the morphology and microstructure of $ZnFe_{1.97}Eu_{0.03}O_4$ nanoparticles, we utilized the SEM and TEM technique to characterize the samples sintered at 750 °C. Figure 2a displayed the corresponding SEM images. We can see that most of the nanoparticles have been aggregated together to form some big rocks with some small particles adsorbed on their surfaces. We further performed the EDS measurement on the sample to analyze the chemical composition, which was shown in the Fig. 2b. Except for the Zn, O and Fe elements, we can obviously observe the weak signal from Eu elements. The

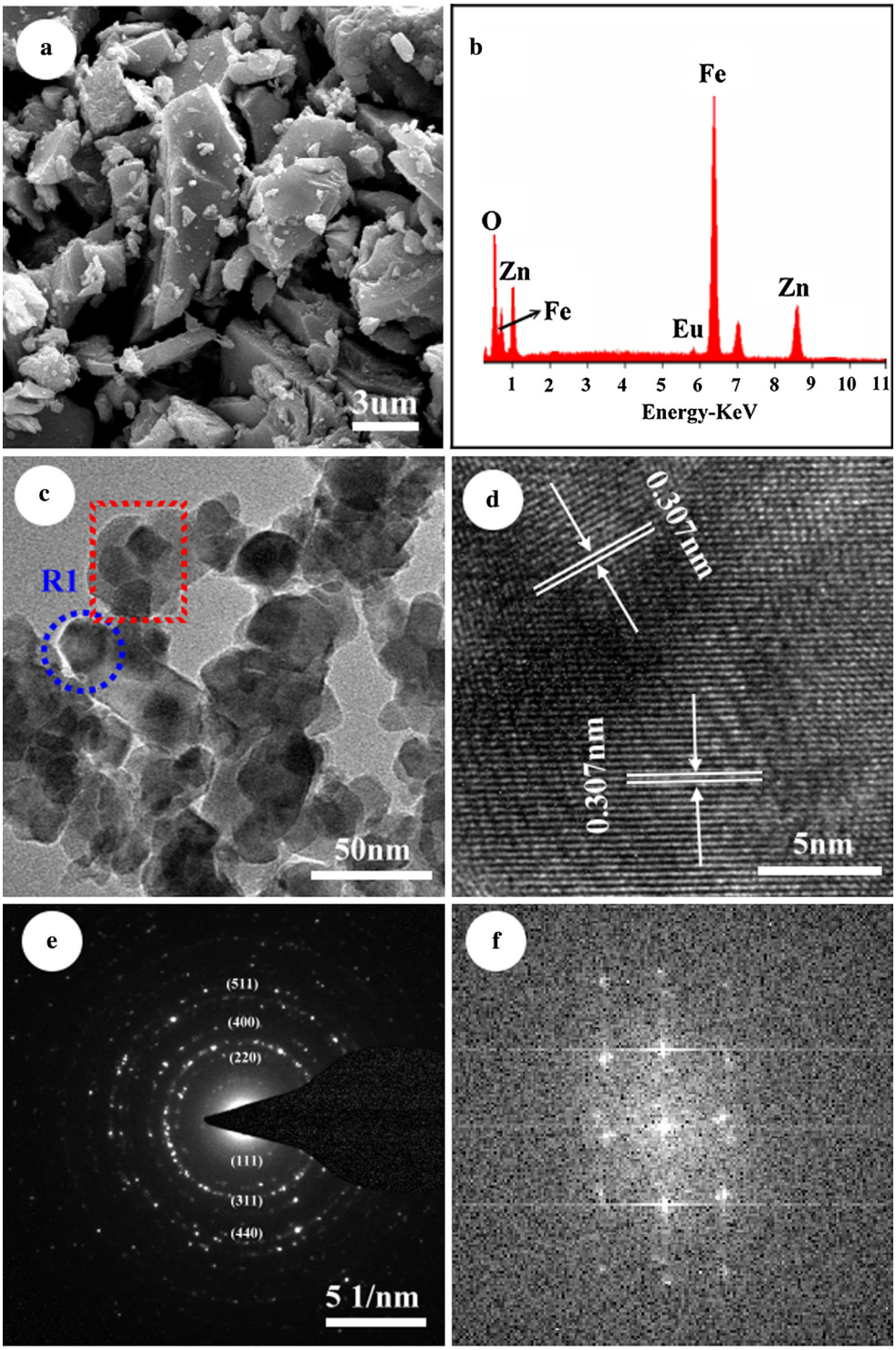

Fig. 2 SEM, EDAX, TEM, HRTEM, SAED and FFT images of the $ZnFe_{1.97}Eu_{0.03}O_4$ nanoparticles sintered at 750 °C

corresponding Eu^{3+} quantitative concentration was estimated to be ~2.39 %, which was smaller than the prospected Eu doping concentration. This could be attributed to the difference of the ionic radius of Fe^{3+} and Eu^{3+} ions. The TEM image was shown in Fig. 2c. We can see that the nanoparticles with irregular shape were aggregated together, especially for the place marked by the red dot rectangle box. The average size was about 20 nm, which was consistent with the XRD results. To make the microstructure clearly, HRTEM images corresponding to the R1 place marked by the blue dot ring in the Fig. 2c was shown in Fig. 2d. The fringe spaces were 0.307 nm, which

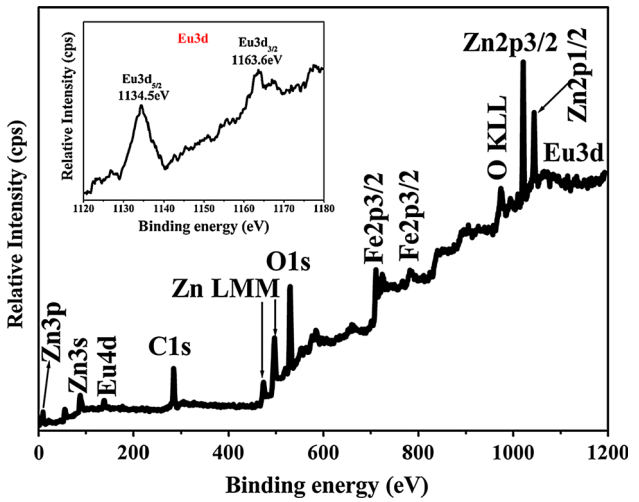

Fig. 3 XPS spectrum of $ZnFe_{1.97}Eu_{0.03}O_4$ nanoparticles sintered at 750 °C. *Inset* shows $Eu3d_{5/2}$ and $Eu3d_{3/2}$ XPS spectrum

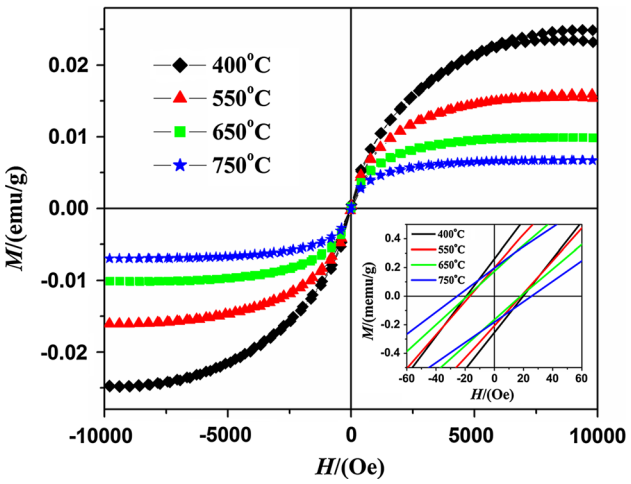

Fig. 4 Magnetic hysteresis loops of the $ZnFe_{1.97}Eu_{0.03}O_4$ nanoparticles sintered at 400, 550, 650 and 750 °C

was corresponding to the (220) plane distance of the standard spinel structure. However, this spacing was bigger than that of standard $ZnFe_2O_4$ (0.298 nm), which was mainly caused by the cell volume expansion when the Eu^{3+} ions doped into $ZnFe_2O_4$ since the ionic radius of Eu^{3+} is much bigger than that of Fe^{3+}. Figure 2e presented the corresponding selected area electron diffraction (SAED) of the sample. The pattern indicated the polycrystalline nature of the sample. The FFT image (Fig. 2f) further proved the result of SAED, in which the few streaky spots might come from the defects in the lattice.

The chemical composition and the binding state of $ZnFe_{1.97}Eu_{0.03}O_4$ had been determined by XPS. Prior to the measurement, the sample was cleaned by an Ar^+ ion etching treatment for 10 s to avoid the effects of surface contamination. The survey scan confirmed the presence of Zn, Fe, O, Eu and C and the absence of other impurities, which confirmed that Eu^{3+} ions successfully incorporated in $ZnFe_2O_4$ lattice. The core-level XPS spectrum of Eu3d was presented in the inset of Fig. 3. The peaks at 1134.5 and 1163.6 eV corresponded to $Eu3d_{5/2}$ and $Eu3d_{3/2}$, respectively [30], which indicated that the Eu ion owns +3 valence in $ZnFe_{1.97}Eu_{0.03}O_4$ nanoparticles [31].

The magnetic properties are the most important properties for ferrites, which are depending on the processing conditions, microstructure, chemical composition and the type of the additives [32, 33]. The room temperature hysteresis loops for the $ZnFe_{1.97}Eu_{0.03}O_4$ nanoparticles sintered at different temperature were shown in Fig. 4. Generally, the $ZnFe_2O_4$ exhibits a paramagnetic behavior, since it is normal spinel, with Zn^{2+} in tetrahedral sites and Fe^{3+} in octahedral sites with antiparallel arrangement of magnetic moments [34]. However, the $ZnFe_{1.97}Eu_{0.03}O_4$ NPs exhibit the weak ferromagnetic behavior. Due to the different number intra-4f shell, Eu^{3+} could lead to the local lattice distortion and lower the formation energy of defects in $ZnFe_2O_4$. These defects created energy levels within the band gap, which presumably hybridized with the 4f levels of RE^{3+} and triggered the onset of magnetic order. These defects also worked as the pinning centers to impede the rotation of the magnetization [35, 36], giving rise to the enhanced coercivity. Therefore, the $Fe_{1.97}Eu_{0.03}O_4$ NPs exhibit the weak ferromagnetic behavior. Moreover, from the hysteresis loops, we can find that the magnetization decreased with the increase of sintering temperature. According to the XRD results, we knew that the grain size of $ZnFe_{1.97}Eu_{0.03}O_4$ nanoparticles enlarged with the increase of sintering temperature. Generally, with the increase of grain size, the defects and local lattice distortion will decrease [5, 37] which finally results in the decrease of magnetization.

4 Conclusions

In summary, we prepared $ZnFe_{1.97}Eu_{0.03}O_4$ NPs with sol–gel method and investigated the effects of sintering temperature on the structural, morphological and magnetic properties. The $ZnFe_{1.97}Eu_{0.03}O_4$ NPs exhibited weak ferromagnetic properties due to the formation of defects in $ZnFe_2O_4$ caused by Eu^{3+} doping. The increased sintering temperature not only enlarged the grain size but also decreased the magnetization of $ZnFe_{1.97}Eu_{0.03}O_4$ NPs due to the decrease of defects in the crystal lattices. Our results not only provide a candidate material for magnetocaloric applications, but inspire people to deeply investigate the rare-earth doped $ZnFe_2O_4$ nanoparticles in both theoretical and experimental aspects.

Acknowledgments The authors would like to acknowledge financial support for this work from China Postdoctoral Science Foundation Grant (Grant Nos. 2011M500863, 2014T70486), Natural Science Foundation of Jiangsu province of China (Item No. BK20130487).

References

1. J.-G. Lee, J.Y. Park, Y.-J. Oh, C.S. Kim, Magnetic properties of $CoFe_2O_4$ thin films prepared by a sol–gel method. J. Appl. Phys. **84**, 2801 (1998)
2. G. Xin, W. Zhu, C. Jia, R. Zhao, W. Schmidt, Y. Wang, Synthesis and microwave absorbing properties of highly ordered mesoporous crystalline $NiFe_2O_4$. Chem. Commun. **47**, 5337–5339 (2011)
3. Y.-L. Liu, Z.-M. Liu, Y. Yang, H.-F. Yang, G.-L. Shen, R.-Q. Yu, Simple synthesis of $MgFe_2O_4$ nanoparticles as gas sensing materials. Sens. Actuators B Chem. **107**, 600–604 (2005)
4. R.A. Candeiaa, M.I.B. Bernardib, E. Longoc, I.M.G. Santosa, A.G. Souza, Synthesis and characterization of spinel pigment $CaFe_2O_4$ obtained by the polymeric precursor method. Mater. Lett. **58**, 569–572 (2004)
5. F.S. Li, H.B. Wang, L. Wang, J.B. Wang, Magnetic properties of $ZnFe_2O_4$ nanoparticles produced by a low-temperature solid-state reaction method. J. Magn. Magn. Mater. **309**, 295 (2007)
6. F. Grasset, N. Labhsetwar, D. Li, D.C. Park, N. Saito, H. Haneda, O. Cador, T. Roisnel, S. Mornet, E. Duguet, J. Portier, J. Etourneau, Synthesis and magnetic characterization of zinc ferrite nanoparticles with different environments: powder, colloidal solution, and zinc ferrite–silica core–shell nanoparticles. Langmuir **18**, 8209 (2002)
7. J.F. Hochepied, P. Bonville, M.P. Pileni, Nonstoichiometric zinc ferrite nanocrystals: syntheses and unusual magnetic properties. J. Phys. Chem. B **104**, 905 (2000)
8. M.K. Roy, H.C. Verma, Magnetization anomalies of nanosize zinc ferrite particles prepared using electrodeposition. J. Magn. Magn. Mater. **306**, 98 (2006)
9. N. Ponpandian, A. Narayanasamy, Influence of grain size and structural changes on the electrical properties of nanocrystalline zinc ferrite. J. Appl. Phys. **92**, 2770 (2002)
10. W.Q. Meng, F. Li, D.G. Evans, X. Duan, Photocatalytic activity of highly porous zinc ferrite prepared from a zinc–iron(III)–sulfate layered double hydroxide precursor. J. Porous Mater. **11**, 97 (2004)
11. R. Zhang, J. Huang, J. Zhao, Z. Sun, Y. Wang, Sol–gel autocombustion synthesis of zinc ferrite for moderate temperature desulfurization. Energy Fuels **21**, 2682 (2007)
12. M. Kobayashi, H. Shirai, M. Nunokawa, Estimation of multiple-cycle desulfurization performance for extremely low-concentration sulfur removal with sorbent containing zinc ferrite–silicon dioxide composite powder. Energy Fuels **16**, 1378 (2002)
13. E. Rezlescu, N. Rezlescu, C. Pasnicu, M.L. Craus, D.P. Popa, The influence of additives on the properties of Ni–Zn ferrite used in magnetic heads. J. Magn. Magn. Mater. **117**, 448–454 (1992)
14. N. Rezlescu, L. Rezlescu, P.D. Popa, E. Rezlescu, Influence of additives on the properties of a Ni–Zn ferrite with low Curie point. J. Magn. Magn. Mater. **215–216**, 194–196 (2000)
15. K. Gheisari, S. Javadpour, H. Shokrollahi, B. Hashemi, Magnetic losses of the soft magnetic composites consisting of iron, and Ni–Zn ferrite. J. Magn. Magn. Mater. **320**, 1544–1548 (2008)
16. R. Gimenes, M.R. Baldissera, M.R.A. da Silva, C.A. da Silveira, D.A.W. Soares, L.A. Perazolli, M.A. da Zaghete, Structural and magnetic characterization of $Mn_xZn_{1-x}Fe_2O_4$ ($x = 0.2$; 0.35; 0.65; 0.8; 1.0) ferrites obtained by the citrate precursor method. Ceram. Int. **38**, 741–746 (2012)
17. M.A. Ahmed, E. Ateia, S.I. El-Dek, F.M. Salem, Rate of heating and sintering temperature effect on the electrical properties of Nd ferrite. J. Mater. Sci. **38**, 1087–1095 (2003)
18. A. Gadkari, T. Shinde, P. Vasambekar, Influence of rare earth ions on structural and magnetic properties of $CdFe_2O_4$ ferrites. Rare Met. **29**(2), 168–173 (2010)
19. N. Rezlescu, E. Rezlescu, C. Pasnicu, M.L. Craus, Effects of the rare-earth ions on some properties of a nickel–zinc ferrite. J. Phys. Condens. Matter **6**, 5707–5716 (1994)
20. X.G. Huang, J. Zhang, H.Z. Wang, S.T. Yan, L.X. Wang, Q.T. Zhang, Er^{3+}-substituted W-type barium ferrite: preparation and electromagnetic properties. J. Rare Earths **28**, 940 (2010)
21. A.B. Gadkari, T.J. Shinde, P.N. Vasambekar, Structural analysis of Y^{3+}-doped Mg–Cd ferrites prepared by oxalate co-precipitation method. J. Mater. Chem. Phys. **114**, 505 (2009)
22. P. Sharma, A. Verma, R.K. Sidhu, O.P. Pandey, Influence of Nd^{3+} and Sm^{3+} substitution on the magnetic properties of strontium ferrite sintered magnets. J. Alloys Compd. **361**, 257 (2003)
23. B.P. Ladgaonkar, C.B. Kolekar, A.S. Vaingankar, Magnetization and initial permeability studies of Nd^{3+} substituted Zn–Mg ferrite system. Bull. Mater. Sci. **22**, 917 (1999)
24. A.M. Samy, Improvement of the magnetic and electrical properties of Cu–Zn ferrites. J. Mater. Eng. Perform. **12**, 569 (2003)
25. S. Komarneni, M.C.D. Arrigo, C. Leonelli, G.C. Pellacani, H. Katsuki, Microwave-hydrothermal synthesis of nanophase ferrites. J. Am. Ceram. Soc. **81**, 3041–3043 (1998)
26. N. Kislov, S.S. Srinivasan, Y. Emirov, E.K. Stefanakos, Optical absorption red and blue shifts in $ZnFe_2O_4$ nanoparticles. Mater. Sci. Eng. B **153**, 70–77 (2008)
27. P.Z. Gao, E.V. Rebrov, T.M.W.G.M. Verhoeven, J.C. Schouten, R. Kleismit, G. Kozlowski, J. Cetnar, Z. Turgut, G. Subramanyam, Structural investigations and magnetic properties of sol–gel $Ni_{0.5}Zn_{0.5}Fe_2O_4$ thin films for microwave heating. J. Appl. Phys. **107**, 044317 (2010)
28. J. Azadmanjiri, Structural and electromagnetic properties of Ni–Zn ferrites prepared by sol–gel combustion method. Mater. Chem. Phys. **109**, 109–112 (2008)
29. A.V. Kadu, S.V. Jagtap, G.N.C. Haudhari, Studies on the preparation and ethanol gas sensing properties of spinel $Zn_{0.6}Mn_{0.4}Fe_2O_4$ nanomaterials. Curr. Appl. Phys. **9**, 1246–1251 (2009)
30. F. Liu, C. Yang, T.L. Ren, A.Z. Wang, J. Yu, L.T. Liu, NiCuZn ferrite thin films grown by a sol–gel method and rapid thermal annealing. J. Magn. Magn. Mater. **309**, 75–79 (2007)
31. M. Veith, M. Haas, V. Huch, Single source precursor approach for the sol–gel synthesis of nanocrystalline $ZnFe_2O_4$ and zinc–iron oxide composites. Chem. Mater. **17**, 95–101 (2005)
32. K. Kondo, T. Chiba, S. Yamada, Effect of microstructure on magnetic properties of Ni–Zn femtes. J. Magn. Magn. Mater. **541**, 254–255 (2003)
33. A.C.F.M. Costa, E. Tortella, M.R. Morelli, R.H.G.A. Kiminami, Synthesis, microstructure and magnetic properties of Ni–Zn femtes. J. Magn. Magn. Mater. **256**, 174 (2003)
34. S. Ayyappan, S.P. Raja, C. Venkateswaran, J. Philip, B. Raj, Room temperature ferromagnetism in vacuum annealed $ZnFe_2O_4$ nanoparticles. Appl. Phys. Lett. **96**, 143106 (2010)
35. J.D. Livingston, A review of coercivity mechanisms. J. Appl. Phys. **52**, 2544 (1981)
36. D. Wang, Q. Chen, G. Xing, J. Yi, S. Rahman Bakaul, J. Ding, J. Wang, T. Wu, Robust room-temperature ferromagnetism with giant anisotropy in Nd-doped ZnO nanowire arrays. Nano Lett. **12**, 3994 (2012)
37. M.A. Valenzuela, P. Bosch, J. Jimenez-Becerrill, O. Quiroz, A.I. Paez, Preparation, characterization and photocatalytic activity of ZnO, Fe_2O_3 and $ZnFe_2O_4$. J. Photochem. Photobiol. A Chem. **148**, 177 (2002)